

## SPARK IGNITION OF TURBULENT METHANE/AIR MIXTURES REVEALED BY TIME-RESOLVED PLANAR LASER-INDUCED FLUORESCENCE AND DIRECT NUMERICAL SIMULATIONS

CLEMENS F. KAMINSKI,<sup>1</sup> JOHAN HULT,<sup>1</sup> MARCUS ALDÉN,<sup>1</sup> STEFFEN LINDENMAIER,<sup>2</sup>  
ANDREAS DREIZLER,<sup>2</sup> ULRICH MAAS<sup>2</sup> AND MARKUS BAUM<sup>3\*</sup>

<sup>1</sup>*Lund Institute of Technology  
Division of Combustion Physics  
S-22100 Lund, Sweden*

<sup>2</sup>*Institut für Technische Verbrennung  
Universität Stuttgart  
Pfaffenwaldring 12, 70569 Stuttgart, Germany*

<sup>3</sup>*C & C Research Laboratories  
NEC Europe Ltd.  
Sankt Augustin, Germany*

By use of high-speed planar laser-induced fluorescence (PLIF) imaging, the evolution of turbulent reactive flows was recorded and studied in real time in a filmlike manner. The technique was used to track the concentration field of the OH radical, which was produced during spark ignition of a turbulent methane/air mixture. The results were compared qualitatively to a two-dimensional direct numerical simulation of the same system using a detailed chemical mechanism and a detailed transport model.

### Introduction

The global effort to optimize industrial power devices has been the major driving force behind modern combustion research. The consumer demand for higher power efficiency, coupled with increasingly strict governmental regulations on pollutant emissions, poses a challenging task to combustion research. One of the most important classes of stationary combustion processes, especially in view of technical applications, is represented by the spark ignition (SI) of reactive mixtures under turbulent flow conditions. In SI engines, for example, the ignition process has a direct bearing on the course of the ensuing combustion cycle. Ineffective combustion in turn leads to pollution and loss of power [1]. Therefore, a detailed understanding of the coupling between chemical and physical processes taking place during ignition is of fundamental interest.<sup>9</sup>

In the past, SI was studied by both numerical and experimental methods. In most cases, experimental studies of SI were carried out in closed vessels and were based on optical methods. In early investigations [2], spark kernels were studied using Schlieren techniques. More recently, the properties of electrical sparks have been related to spectroscopically measured temperatures and interferometric observations of the flow field [3–5]. Bradley et al. studied

spark ignition and turbulent burning velocities in gaseous mixtures in a fan-stirred bomb using fast photography [6,7]. Laser-based techniques also were applied to investigate the shape of flame kernels [8] as well as the temporal development of flame initiation [9]. Several researchers have investigated the influence of spark energy on the kernel structure [10–12]. The development of the flame kernel depends strongly on the gap between the electrodes and on the electrode diameter, as shown experimentally [8] and numerically [13,14]. Furthermore, the electrodes shape [15,16] and the flow field influences the development of the flame kernel [17–19]. Heat loss to the electrodes, sometimes responsible for flame quenching, was also the subject of several investigations [20–22].

In the present paper, we describe a detailed study of the growth of a spark-ignited flame kernel and the transition from laminar to turbulent flame development. The electrical spark was produced by a well-characterized and reproducible ignition system [9]. We used planar laser-induced fluorescence (PLIF) [23,24] sequenced at high repetition rates to track the evolution of the OH radical produced during the ignition of homogeneous mixtures of methane (CH<sub>4</sub>) and air subjected to varying degrees of controlled turbulence. This approach allowed the tracking of intermediate species taking place in a turbulent flow in a filmlike manner [25]. Furthermore, we present a full two-dimensional direct numerical simulation

\*Current address: Daimler Chrysler AG, FTS, HPC 0522, D-70546 Stuttgart, Germany.

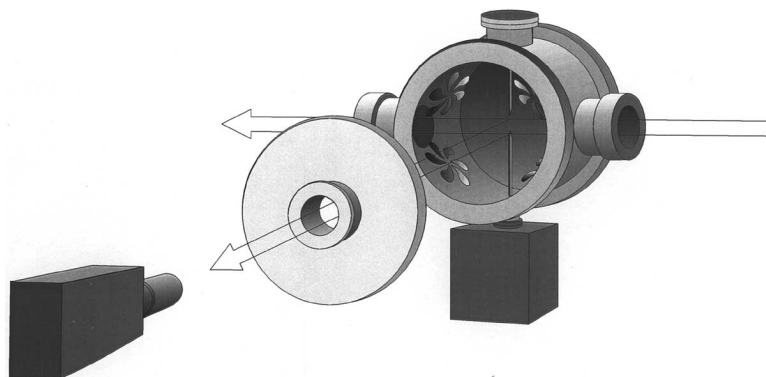


FIG. 1. Drawing of the ignition cell for turbulence/chemistry interaction studies.

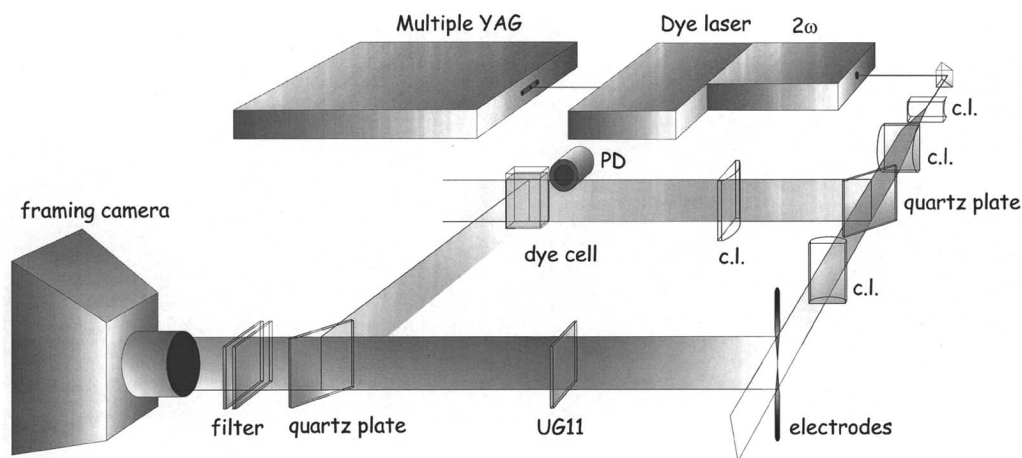


FIG. 2. Schematic setup for the PLIF experiments.  $2\omega$ : frequency doubling unit, PD: Photodiode, c.l.: cylindrical lens; UG11: filter to reject laser stray light.

(DNS) calculation for the same system. The approach was based on a detailed chemical reaction mechanism and a comprehensive transport model. The detailed study of the interaction of turbulence and chemistry is possible with the current approach. Additionally, the approach presented in this paper may help to develop improved models necessary for the statistical description of turbulent combustion.

### Methodology

A schematic representation of the reaction vessel used for the present studies is shown in Fig. 1. Two sharpened tungsten electrodes, separated by a distance of 1 mm, were centered in the cell and used to ignite homogeneous methane/air mixtures. The spark duration and energy content were controlled by rapid adaptive regulation of the voltage between the electrodes according to the plasma resistance,

which dropped as the spark channel developed, due to the production of ionized species. Details of the SI system can be found in Ref. [9]. Controlled amounts of turbulence were coupled into the mixture via four high-speed rotors situated at a radial distance of 200 mm from the electrode gap. Rotor speeds were adjusted between 0 and 5000 revolutions per minute (rpm), corresponding to turbulence intensities ranging from 0 to  $4 \text{ ms}^{-1}$  as measured by laser Doppler anemometry in a fan-stirred vessel of similar geometry [26].

A schematic representation of the setup used for the PLIF experiments is shown in Fig. 2. OH was excited using the temperature insensitive  $Q_1(8)$  transition in the  $A^2\Sigma^+ \leftarrow X^2\Pi$  electronic band in the 282 nm wavelength region. The exciting laser pulses were obtained using the frequency doubled output from a dye laser (Continuum) operating near 564 nm on Rhodamine 590 dye. The dye laser was pumped by light pulses from the frequency doubled output

of four individual Nd:YAG lasers (BMI). The pump pulses were combined into a single beam before entering the dye laser with separations between individual pulses typically of order 1 ms. The laser light was formed into a sheet of 50 mm in height and  $160 \pm 30 \mu\text{m}$  in width by a cylindrical telescope. The light sheet was passed through the cell via two quartz windows passing about 1 mm away from the electrodes (see Fig. 1). Subsequent fluorescence was imaged onto a specially designed fast framing camera (Hadland Photonics). The camera consisted of eight intensified CCD cameras (ICCD) arranged in a circular fashion around a common optical input axis. The light entering the camera was directed to the individual channels by an eight-facet pyramid beam-splitter. Time resolution was achieved by sequentially gating the ICCD channels synchronously with the laser pulse sequence. Two microseconds after each PLIF image, a corresponding OH-chemiluminescence image was recorded to obtain additional structural information on the flame kernel (see discussion further below). This  $2 \mu\text{s}$  time delay was necessary to avoid crosstalk between the channels recording PLIF and chemiluminescence and can be considered instantaneous on the turbulence and overall chemistry timescales. Exposure times were 200 ns for PLIF and  $30 \mu\text{s}$  for the much weaker emission images.

The DNS calculations were performed using the program NSCORE [27]. The fully compressible Navier-Stokes equations were solved in two dimensions, including multicomponent transport models, Soret effect (mass diffusion caused by temperature gradients), and Dufour effect (temperature diffusion by concentration gradients). This two-dimensional approach made it computationally feasible to include detailed chemistry. Since the DNS covered all occurring timescales, information on the coupling between turbulence and chemistry became available in complete detail. Flame stretching and curvature as well as Lewis number effects (caused by differences between thermal and mass diffusion) could also be studied over a wide parametric range. Although it is recognized that two-dimensional turbulence differs from three-dimensional turbulence, the response of the flame front during its growth can be assumed to be generic [28], even though detailed statistical correlations of small scale quantities may differ. Future investigations will focus on full three-dimensional calculations using complex chemistry, although statistical studies may still have to be based on two-dimensional calculations because of prohibitive computational times. Numerically the governing equations were solved using a high-order compact scheme with a minimum of dissipation for the discretization of derivatives and a Runge-Kutta method for time advancement. Details can be found in Refs. [29,30]. To investigate turbulent flames with complex chemistry, reliable elementary reaction mechanisms are required. In the present case, a detailed

$\text{CH}_4$  oxidation scheme developed by Warnatz [31] was employed, including 17 species and 52 reactions. The computational domain was a square box of approximately  $1 \times 1 \text{ cm}^2$  in which an initially homogeneous mixture of cold, unburned reactants was present. Homogeneous isotropic turbulence of type “von Karmann-Pao” [32] was superimposed on the initial mixture. The spark was modeled by inclusion of a source term in the energy conservation equation with a Gaussian radial profile, located in the middle of the computational domain, a similar approach as used in Ref. [9].

## Results

Figure 3a–c shows temporal PLIF sequences of single ignition events corresponding to the evolution of the OH concentration field. Fig. 3d corresponds to direct OH-chemiluminescence emission recorded “simultaneously” with the OH-PLIF sequence shown in (c). The rotor speeds are 0 (a), 1000 (b), and 3000 rpm (c and d), respectively. The width of each image shown corresponds to 40 mm. Fuel mixtures were stoichiometric in all cases. Sequence 3a corresponds to the laminar flame propagation case when the fans are not rotating. The OH concentration scales were obtained by calibrating the relative PLIF intensities against one-dimensional laminar flame calculations including full  $\text{CH}_4$  chemistry [9]. The loss of signal by molecular collisions was assumed constant throughout the measurement region. This is a reasonable assumption with the given variation of temperature and concentrations in the combustion product zone [33]. Errors in the concentrations shown are estimated to be  $\pm 30\%$ , including contributions from measurement uncertainties and computational errors. Surface effects on the chemical reaction, caused by heat loss and radical recombination near the electrode surface, are clearly visible: The propagation speed of the reaction is slower along the axis defined by the electrodes, and the OH radical concentration drops drastically in the electrodes’ vicinity (blue regions, last two images of the sequence in Fig. 3a).

At 1000 rpm, Fig. 3b, the flame exhibits an increased degree of wrinkling caused by turbulent eddies. As a consequence, the reaction surface area (defined by the interface between unburned reactants and burnt products) is increased and the chemical reaction is speeded up (evident from the shorter time delay between exposures in the sequence). At 3000 rpm, Fig. 3c, isolated structures appear in the PLIF images. The chemiluminescence in Fig. 3d corresponds to the sequence shown in Fig. 3c. As chemiluminescence imaging is a line-of-sight technique and integrates through the light emitting volume, structural information on the flame, such as wrinkling and eddy formation, which are clearly exhibited by the PLIF images, cannot be recovered.

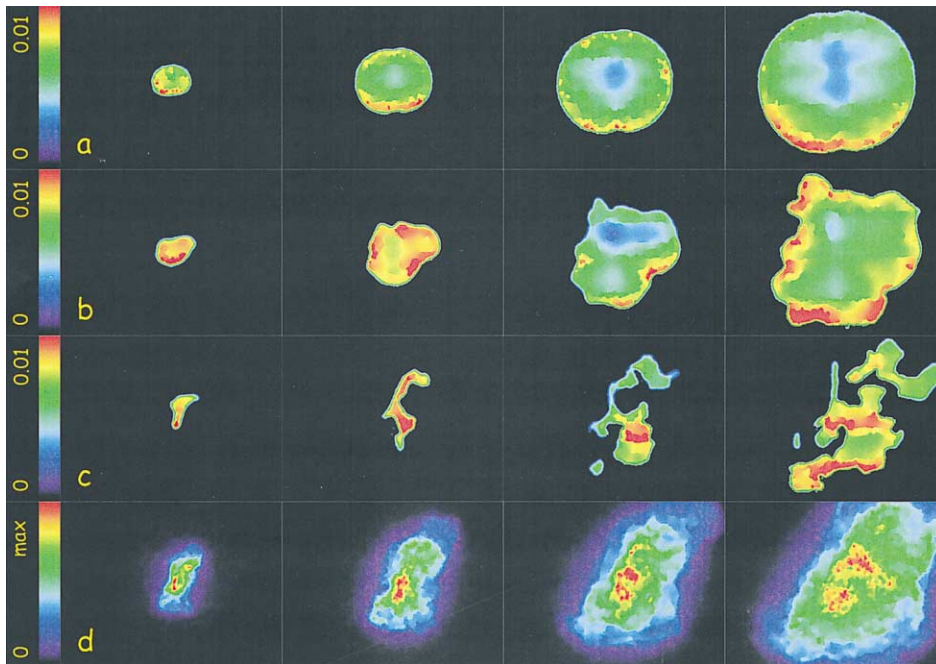


FIG. 3. Evolution of OH concentration fields for three different ignition events corresponding to rotor speeds of 0 (a), 1000 (b), and 3000 rpm (c and d). In (d), line-of-sight chemiluminescence of OH is shown which corresponds to the PLIF sequence shown in (c). In (a), the pictures correspond to 1.5, 3.5, 5.5, and 7.5 ms after spark occurrence. In (b), the times are 1.5, 3.2, 4.9, and 6.6 ms, respectively. In (c) and (d), times correspond to 1.5, 2.6, 3.7, and 4.8 ms. The color scales correspond to the species mole fractions. In (d), the scale is in arbitrary units.

However, taken “simultaneously,” the two techniques provide considerable topological information on the local structure of the combustion process. Statistical information can be gathered both on the evolution of the surface area (from the PLIF data) and the reaction volume (from chemiluminescence). Flame speed and stretch and strain rates are available, and the data are ideally suited for comparisons with numerical experiments.

The regimes of turbulence/chemistry interactions are conveniently classified by comparing the characteristic chemical and turbulent time and length scales of the system. A possible classification for turbulent premixed combustion can be made in terms of the turbulent Reynolds number  $Re_T$  and the turbulent Karlovitz number  $Ka_T$  based on the so-called Borghi diagram [34]. The Karlovitz number

$$Ka_T = \frac{\delta_{LZ}^2}{l_k^3} \quad (1)$$

relates the thickness of the reaction layer  $\delta_{LZ}$  in the laminar flame to the Kolmogorov length scale  $l_k$ , which states the size of the smallest possible eddies in the flow (the size at which molecular transport processes dissipate turbulent structures instantaneously). In contrast, the turbulent Reynolds number

$$Re_T^{3/4} = \frac{l_0}{l_k} \quad (2)$$

relates the size  $l_0$  of the largest to the smallest eddies present in the flow. Fig. 3a corresponds to  $Re_T < 1$ , which is in the laminar flame regime on the Borghi diagram. In Fig. 3b,  $Re_T = 272$  and  $Ka_T = 2.44$ . This regime corresponds to a region close to the so-called laminar flamelet regime [35]. Here, the flame burns in thin, laminar-flame-like layers, which are stretched and wrinkled by turbulence, whereas the principle structure is not changed by turbulence. The flamelet assumption offers significant computational advantages because information obtained for laminar flames can be directly used for the description of turbulent flames [36]. In Otto engines, for example, the flamelet assumption has often been found to be valid for low and midrange speeds [37]. However, the precise range of validity of this approach is a matter of debate, and more experimental data and theoretical efforts are needed. In Fig. 3c, the respective numbers are  $Re_T = 816$  and  $Ka_T = 12.75$ . This is an example which shows how turbulence disrupts or even extinguishes laminar flamelets. In this regime, detailed information is of special significance because the interaction of turbulence

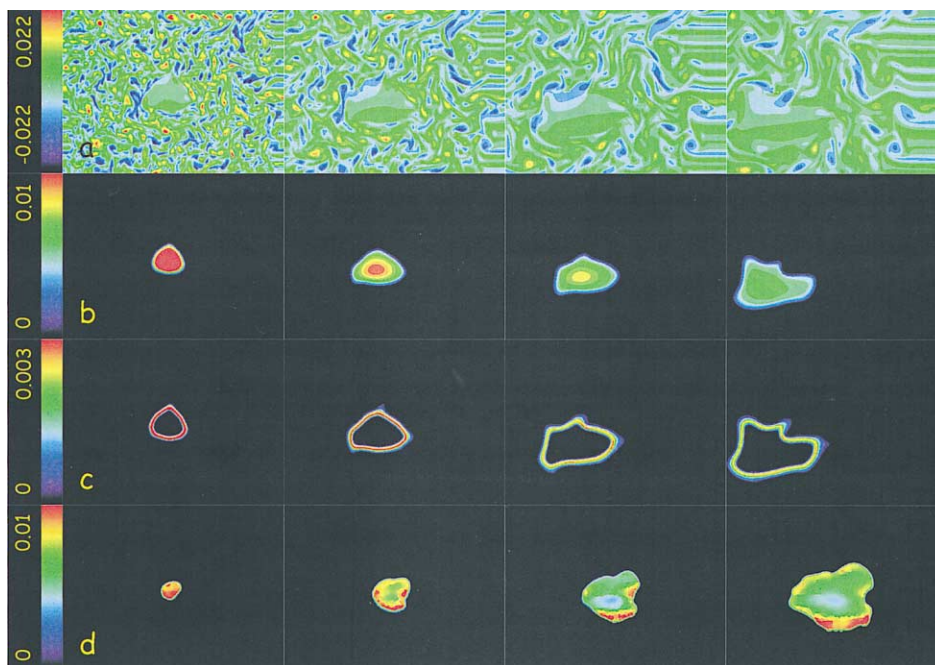


FIG. 4. DNS calculations showing the evolution of (a) vorticity field ( $\text{s}^{-1}$ ), (b) OH concentration field (molar fraction), and (c) formaldehyde concentrations ( $\text{CH}_2\text{O}$ , molar fraction). The timescale going from left to right in each sequence corresponds to  $t/\tau = 0.3, 0.6, 0.9,$  and  $1.2$ , respectively. In (d) an OH-PLIF sequence obtained under similar conditions is shown (molar fraction).

and chemical kinetics can lead to a structural change of the reaction layer.

A DNS calculation is shown in Fig. 4. In Fig. 4a, the vorticity field (corresponding to a turbulence intensity of  $u' = 3 \text{ ms}^{-1}$ ) as a function of time is shown. The evolution of the OH and  $\text{CH}_2\text{O}$  (formaldehyde, an important marker of the flame front [38]) concentration fields are shown as examples (Fig. 4b and c, respectively). An experimentally obtained PLIF sequence of OH is shown in Fig. 4d for comparison. The time steps are given in units of  $t/\tau$ , where  $\tau$  is the turnover time of the most energetic eddies in the flow. The scale for the color of the contour levels is fixed throughout each sequence. The influence of turbulence on the chemistry can be clearly tracked in the sequence. At about half the turnover time ( $t/\tau = 0.6$ ), the first negatively curved features appear on the flame front, revealing the onset of turbulence chemistry interactions since in laminar flames only positive curvatures are observed [9]. At  $t/\tau = 1.2$  (corresponding to about  $500 \mu\text{s}$  after the spark), the flame has reached the boundary of the computational domain. It exhibits significant wrinkling and a largely increased surface area compared with a laminar flame. Nevertheless, the flame front is still continuous and the turbulent flame is still well described as an ensemble of laminar flamelets.

Note the high levels of OH in the beginning of the sequence caused by the large temperatures prevailing initially during the electrode discharge ( $t/\tau = 0.3$ ). This peak is rapidly leveling out to equilibrium concentrations as the flame starts to propagate. Fig. 4a shows the effects of chemistry on the turbulence: The velocity fluctuations (which are related to the vorticity) are significantly dissipated in the burnt gas region. This phenomenon is caused not only by the higher viscosity of the products, which is about a factor of 4 larger compared with the unburned reactants, but also by the lower density of the hot products. The vorticity field corresponding to the shown calculation exhibits a net velocity component to the left of the imaged plane responsible for the global movement of the flame kernel. In the calculation, turbulence is continuously decaying via viscous dissipation. This decay is not observed in the physical experiment since here the turbulence field is continuously fed by the rotating fans. Although the effect of this on the flame kernel is small for the short flame propagation times presented here, this shows a limitation of DNS. However, direct modeling of the whole system including the rotating fans in combination with detailed chemistry schemes is not possible with the computational resources available today.

### Discussion and Concluding Remarks

A large experimental database has been set up as a result of the present work regarding the temporal evolution of ignition under various conditions. PLIF/chemiluminescence data are available for a range of parameter sets (stoichiometry, speed of the fans, temporal resolution, ignition characteristics), and 32 individual ignition events have been recorded per set. This large collection of experimental results will serve as the basis for a statistical analysis yielding means and fluctuations of lengths of flame fronts, areas of burned gases, surface to volume ratios, and curvatures. Efficient schemes for effective data reduction and batch postprocessing of images are currently being developed for this task [39,40].

For a more detailed comparison between the calculations and the PLIF experiments, runs on larger computational domains than shown (currently limited to  $1 \times 1 \text{ cm}^2$ ) are required. Two-dimensional DNS are currently in progress on  $4 \times 4 \text{ cm}^2$  domains. Similar to experimental investigations, a repetition of DNS calculations is necessary to obtain statistically representative information. Thus, DNS calculations will be repeated several times using fixed initial and boundary conditions chosen in agreement with experimental characteristics.

Although the extent to which this will be possible is limited by available computational resources, such detailed investigations of the coupling process between chemistry and turbulence still serve as an important tool to improve simplified turbulence models which are used in computational fluid dynamics (CFD) calculations of practical combustion processes. These methods rely on models which are based on statistical quantities. In the flamelet-based approaches, for example, Ref. [35], propagation equations for the flame surface are solved. These models need information on average rates of propagation, surface generation, and so on, which can be obtained from the type of research presented here. On the other hand, probability density function models for reacting flows [41] rely on mixing models for the unclosed conditional expectations of the molecular fluxes, that is, information on gradient correlations. Improvement of both approaches can also be guided by both experiments and DNS.

In conclusion, this report shows the potential of state-of-the-art experimental and numerical techniques to follow the evolution of complex chemical reactions subjected to a turbulent flow field in real time. Two-dimensional concentration fields of a short-lived combustion-produced radical were measured in a filmlike manner for the first time by temporally resolved PLIF. A large experimental database is available and is going to be analyzed with respect to statistical quantities using advanced image postprocessing. On the other hand, DNS calculations employing larger computational domains are in

progress. PLIF data combined with numerical simulations can provide the basis for the validation of combustion models, which can then be used in the design of technical combustion processes.

### Acknowledgments

This work was supported by a grant under the EU TMR programme "Access to Large Scale Facilities," contract number ERBFMGECT950020(DG12), which is gratefully acknowledged.

### REFERENCES

1. DeCicco, J., and Ross, M., *Sci. Am.* 12:30–35 (1994).
2. Olsen, H. L., Edmonson, R. B., and Gayhart, E. L., *J. Appl. Phys.* 23:1157 (1952).
3. Maly, R., and Vogel, M., *Proc. Combust. Inst.* 17:821 (1979).
4. Maly, R., Saggau, B., Wagner, E., and Ziegler, G., SAE technical paper 83-0478.
5. Ziegler, G., Wagner, E., and Maly, R., *Proc. Combust. Inst.* 20:1817 (1984).
6. Akindele, O. O., Bradley, D., Mak, P. W., and McMahon, M., *Combust. Flame* 47:129–155 (1982).
7. Abdel-Gayed, R. G., and Bradley, D., *Proc. Combust. Inst.* 16:1725–1735 (1976).
8. Xu, J., Behrendt, F., and Warnatz, J., *Proc. COMODIA* 69–73 (1994).
9. Dreizler, A., Lindenmeier, S., Maas, U., Hult, J., Aldén, M., and Kaminski, C. F., *Appl. Phys. B* 70:287–294 (2000).
10. Bradley, D., and Lung, F. K.-K., *Combust. Flame* 47:71–93 (1987).
11. Lim, M. T., Anderson, R. W., and Arpaci, V. S., *Combust. Flame* 69:303–313 (1987).
12. Pischinger, S., and Heywood, J. B., SAE technical paper 88-0518.
13. Ishii, K., Tsukamoto, T., Ujiiie, Y., and Kono, M., *Combust. Flame* 91:153–164 (1992).
14. Kono, M., Ishii, K., Niu, K., and Tsukamoto, T., *Prog. Astronaut. Aeronaut.* 131:55–70 (1991).
15. Pitt, P. L., Clements, R. M., and Topham, D. R., *Combust. Sci. Technol.* 78:289–314 (1991).
16. Kono, M., Niu, K., Tsukamoto, T., and Ujiiie, Y., *Proc. Combust. Inst.* 22:1643–1649 (1988).
17. Kravchik, T., Sher, E., and Heywood, J. B., *Combust. Sci. Technol.* 108:1–30 (1995).
18. Borghese, A., Diana, M., Moccia, V., and Tamai, R., *Combust. Sci. Technol.* 76:219–231 (1991).
19. Akram, M., *AIAA J.* 34(9):1835–1842 (1996).
20. Thiele, M., Warnatz, J., and Maas, U., SAE technical paper 99-01-1178.
21. SAE technical paper 90-0021.
22. Ko, Y., and Anderson, R. W., SAE technical paper 89-2083.
23. Kychakoff, G., Howe, R. D., and Hanson, R. K., *Science* 224:382–384 (1984).

24. Yin, B., Lam, J. K., Winter, M., and Long, M. B., *Science* 235:1209–1211 (1987).
25. Kaminski, C. F., Hult, J., and Aldén, M., *Appl. Phys. B* 68:757–760 (1999).
26. Nastoll, W., Dissertation, University of Karlsruhe, Engler-Bunte-Institut, 1989.
27. Baum, M., “Direct numerical simulation: A tool to study turbulent reacting flows,” in *Annual Reviews of Computational Physics, Vol. V*, World Scientific Publishing Company, Singapore, 1997, pp. 25–95.
28. Poinso, T. J., “Flame ignition in a premixed turbulent flow,” in *Annual Research Briefs*, Center for Turbulent Research, Stanford Univ./NASA-Ames, Stanford, CA, 1991, pp. 251–272.
29. Baum, M., Poinso, T. J., Haworth, D., and Darabiha, N., *J. Fluid. Mech.* 281:1–32 (1994).
30. Baum, M., Poinso, T. J., and Thévenin, D., *J. Comput. Phys.* 116:247–261 (1995).
31. Warnatz, J., *Combust. Sci. Technol.* 64:34–177 (1983).
32. Hinze, J. O., *Turbulence*, McGraw-Hill, New York, 1975.
33. Buschmann, A., Dinkelacker, F., Schäfer, T., and Wolfrum, J., *Proc. Combust. Inst.* 26:437–445 (1996).
34. Borghi, R., in *Recent Advances in Aeronautical Science*, Pergamon, London, 1985, pp. 117–134.
35. Peters, N., *Turbulent Combustion*, Cambridge University Press, Cambridge, 1999.
36. Candel, S., Veynante, D., Lacas, F., and Darabiha, N., *Combust. Sci. Technol.* 98:245 (1996).
37. Becker, H., Arnold, A., Suntz, R., Monkhouse, P., Wolfrum, J., Maly, R., and Pfister, W., *Appl. Phys. B* 50:473–478 (1990).
38. Paul, P. H., and Najm, H. N., *Proc. Combust. Inst.* 27:43–50 (1998).
39. Malm, H., Sparr, G., Hult, J., and Kaminski, C. F., *J Opt Soc Am A17*, in press (2000).
40. Schiessl, R., Dreizler, A., and Maas, U., SAE technical paper 99-01-3651.
41. Pope, S. B., *Prog. Energy Combust. Sci.* 11:119 (1986).

## COMMENTS

*Rainer Suntz, University of Karlsruhe, Germany.* The two-dimensional maps of the OH-concentration distribution obtained by DNS and PLIF-measurements deviate from each other. Can you give an explanation for these deviations?

*Author's Reply.* It should be noted that a direct comparison between individual experimental runs and DNS calculations is not permissible because of the stochastic nature of the process. Such a comparison can be conducted only on a statistical basis. However, qualitatively the characteristics of the developing flame kernels are similar in nature, for example, the onset and character of flame wrinkling, and the initial high OH concentration peak near spark initiation. In the DNS, the OH concentration in the center of the ignition kernel decreases slowly in time due to diffusion, chemical reaction, and heat conduction. On the other hand, in the experiments the peak OH concentration in the center of the flame kernel vanishes rapidly. This can be attributed in particular to the effect that the experiments yield concentrations along a two-dimensional sheet of the three-dimensional flame kernel which typically does not contain the point of the initial energy deposition (due to the offset of the laser sheet from the electrodes and due to the random displacement of the flame kernel caused by turbulence). One additional minor effect is that

heat conduction to the electrodes present in the experiments is not accounted for in the corresponding DNS. In laminar ignition cases performed with the present setup, quantitative comparisons reveal good agreement between measurements and simulations for all cases studied, except in the vicinity of the electrodes [1].

## REFERENCE

1. Dreizler, A., Lindenmaier, S., Maas, U., Hult, J., Aldén, M., and Kaminski, C. F., *Appl. Phys. B* 70:287–294 (2000).



*James Kelman, Cranfield University, UK.* Could the authors comment on the difference in structure of the OH presented in their images, particularly the difference between the experimental and the DNS results? While the experimental results show typical premixed flame propagation with high OH concentration at the flame front, the DNS results show the opposite. The OH concentration appears to peak in the center of the flame kernel, and even the image with the longest delay after ignition shows no evidence of high OH at the propagating flame front.

*Author's Reply.* Same reply as above.